Environmental Research Communications

LETTER

Reconstruction of sea ice variability in the Chukchi Sea during the last three centuries based on biomarker proxies

Bassem Jalali[1,2], **Marie-Alexandrine Sicre**[3], **Jian Ren**[1,2], **Vincent Klein**[3], **Zhongqiao Li**[1,2], **Liang Su**[1,2], **Youcheng Bai**[1,2], **Anatolii S Astakhov**[4] and **Jianfang Chen**[1,2,5,*]

[1] Key Laboratory of Marine Ecosystem Dynamics, Second Institute of Oceanography, Ministry of Natural Resources, Hangzhou 310012, People's Republic of China
[2] Second Institute of Oceanography, Ministry of Natural Resources, Hangzhou 310012, People's Republic of China
[3] LOCEAN, CNRS, Sorbonne Université, Campus Pierre et Marie Curie, Case 100, 4 Place Jussieu, 75032, Paris, France
[4] V.I. Il'ichev Pacific Oceanological Institute, Far Eastern Branch of Russian Academy of Sciences, Vladivostok, Russia
[5] State Key Laboratory of Satellite Ocean Environment Dynamics, Second Institute of Oceanography, Ministry of Natural Resources, Hangzhou 310012, People's Republic of China
* Author to whom any correspondence should be addressed.

E-mail: jfchen@sio.org.cn

Keywords: biomarkers, IP_{25}, PIP_{25}, pre-Industrial Era, Arctic Ocean

Supplementary material for this article is available online

OPEN ACCESS

RECEIVED
26 April 2024

REVISED
19 August 2024

ACCEPTED FOR PUBLICATION
30 August 2024

PUBLISHED
23 September 2024

Abstract

In this study, we reconstruct three-century of sea ice cover history in the Chukchi Sea from the downcore profile of total organic carbon (TOC) and biomarker proxies, namely the Ice Proxy with 25 carbon atoms (IP_{25}), the di- and tri-unsaturated highly branched isoprenoid (HBI II and HBI III) and two phytosterols (brassicasterol and dinosterol) in three sediment cores from the northern, eastern and southern Chukchi Sea reflecting different sea ice conditions. Our data indicate higher IP_{25} values in the eastern site and lowest ones in the northern Chukchi Sea site that are consistent with the modern sea ice distribution. They also underline the predominance of sympagic over pelagic production except at the southern site where pelagic production depicts a sharp increased over the last decades. We present a new approach improving the linear relationship between $P_{III}IP_{25}$ (P_BIP_{25}) and satellite-derived spring (summer) sea ice concentrations (SIC) to advance sea ice reconstructions across the Arctic Ocean. This method results in better assessment of PIP_{25} derived SIC and reconstruction of past seasonal sea ice conditions. They indicate marginal sea ice conditions at the three sites until 1950s–1960s followed by a reduction of seasonal sea ice as captured by P_BIP_{25} index.

1. Introduction

Climate change is the major challenge for the world population of the 21st century that requires urgent mitigation and adaptation actions to be taken (Calvin et al. 2023). The Arctic region is a key component of the global climate system and a hotspot of climate change due to polar amplification (Bernstein *et al* 2008). Over the last four decades, the Arctic Ocean has experienced a dramatic reduction of sea ice extent, thickness and volume that is most pronounced in late summer (Perovich *et al* 2019). Remote sensing data between 1979 and 2020 evidence a decrease of sea ice extent by 13.1% per decade in summer (September) and by 2.2% per decade in winter (March) (Perovich *et al* 2019). Sea ice thickness and volume as well as the multiyear ice extent (e.g. the sea ice that survives at least one summer melting) have also considerably reduced (Kwok and Rothrock 2009, Tschudi *et al* 2016, Perovich *et al* 2019). These declines are due to several factors among which the increase of sea surface temperature (Timmermans and Labe 2020), surface air temperature (Ballinger *et al* 2020), radiative forcing and near surface winds, which are among the strongest on Earth (Ogi *et al* 2010, Kapsch *et al* 2016). Winds indeed facilitate heat transfer within the ocean interior and contribute to sea ice cover decline through dynamical air-sea processes as sea ice thins and becomes more exposed to wind forcing. The atmospheric

Table 1. Location of short sediment cores from the Arctic region with average PIII-IP_{25} and PB-IP_{25} during the remote sensing period and corresponding average seasonal SIC from satellite data (1979–2017).

Cores	Lat. (°North)	Lon. (°East)	Water depth (m)	PIII IP_{25}[a]	PIII IP_{25} (c = 1)	PB IP_{25}[a]	SpSIC (%)[b]	SuSIC (%)[b]	Sp-SuSIC (%)[b]	References
DA17-NG-ST08-090R	78.5	−17.307	595	NA	NA	0.60	99.11	90.94	95.03	Davies *et al*
BASICC 8	77.98	26.79	135	0.49	0.95	NA	88.10	11.98	50.04	Köseoğlu *et al* 2018
DA17-NG-ST10-109R	77.95	−15.493	503	NA	NA	0.62	98.14	67.21	82.68	Davies *et al*
DA17-NG-ST12-134R	77.125	−10.663	501	NA	NA	0.41	95.09	50.45	72.77	Davies *et al*
ARC11-R1	74.64	−169.13	200	0.49	0.54	0.44	98.99	62.79	80.89	Su *et al* 2023
14R09	74.61	−168.98	184	0.56	0.96	0.44	99.00	62.53	80.76	This study
ARA01B-03MUC	73.52	−168.94	72.5	0.64	0.96	0.46	98.90	56.94	77.92	Kim *et al* 2019
BASICC 1	73.1	25.63	425	0.00	0.00	NA	0.00	0.00	0.00	Köseoğlu *et al* 2018
ARC4-C07	72.54	−165.33	51	0.50	0.92	0.48	98.44	38.69	68.56	Bai *et al* 2022
BASICC 43	72.54	45.74	285	0.39	0.14	NA	11.03	0.00	5.51	Köseoğlu *et al* 2018
R406MC032	72.32	15.38	1035	0.00	0.00	NA	0.00	0.00	0.00	Belt *et al* 2019
14S03	72.23	−157.05	172	0.39	0.90	0.49	97.81	37.55	67.68	This study
R248MC010	70.31	12.88	1254	0.00	0.00	NA	0.00	0.00	0.00	Belt *et al* 2019
LV77-4	69.2	−174.9	60	0.30	0.59	0.36	90.64	7.90	49.27	This study

[a] c value is calculated from biomarker data of each core

[b] Average SIC values at each core site are calculated for the period between 1979 and 2017.

circulation, primarily controlled by the Arctic Oscillation (AO), also plays a part in sea ice reduction by flushing out thick ice in winter across Fram Strait resulting in thinner winter ice pack. Furthermore, Ogi *et al* (2010) have shown that anticyclonic circulation over Beaufort Sea in summer enhances sea ice export into the Atlantic Ocean thereby affecting the thermohaline circulation through freshwater export to convection sites of the North Atlantic, with probable consequences on the global climate (van Westen *et al* 2024). Finally, it has been shown that these changes in the Arctic Ocean are already altering polar ecosystems (Coupel *et al* 2012, 2015, Lee *et al* 2019, Zhuang *et al* 2020). For instance, chlorophyll-a observations from remote sensing show higher primary productivity between 2003 and 2020 across all regions of the Arctic Ocean primarily because of sea ice cover shrinking and longer growing season of phytoplankton, impacting on the carbon cycle (Frey *et al* 2021).

Data on secular sea ice conditions in the subpolar and polar Pacific Arctic Region (PAR) are still insufficient to fully understand the response of sea ice to the emergence of global warming dated around 1860 (Abram *et al* 2016, McCulloch *et al* 2024). Only few paleo-sea ice reconstructions based on biomarkers exist in the polar PAR (Kim *et al* 2019, Hu *et al* 2020, Bai *et al* 2022, Su *et al* 2023) and therefore sea ice changes at regional scale are still largely under documented, limiting reliable prediction of environmental conditions and marine resources in the region. In order to place the satellite observations into a longer perspective and better evaluate on-going changes, we analyzed sea ice proxies in three marine sediment cores in the Chukchi Sea to reconstruct the decadal variability and mid- to long-term trends of Arctic sea ice prior to atmospheric CO_2 rise caused by human activities.

In this study, we combine sympagic phytoplankton biomarkers, e.g. the mono- and di-unsaturated Highly Branched Isoprenoids (HBIs), IP_{25} and HBI II respectively (Belt *et al* 2007, Brown *et al* 2014), with open-water pelagic phytoplankton biomarkers e.g., HBI III, brassicasterol and dinosterol, measured in three marine sediment cores of the Chukchi Sea to reconstruct past sea ice conditions. These data are used to calculate PIP_{25} indexes (Müller *et al* 2011) and derive sea ice cover estimates and reconstructions at three sites, two of them extending back into the pre-industrial period. We compare these reconstructions against satellite and historical data as well as existing paleo-records to evaluate the temporal evolution of sea ice cover in the Chukchi Sea since the beginning of the Industrial Era.

2. Materials

2.1. Sediment cores

Three sediment multi-cores were retrieved from areas exposed to different sea ice conditions of the Chukchi Sea (East, South and North) to be analyzed for biomarkers. Core 14S03 (72.23°N, 157.05°W; 51 cm long, 172 m water depth) and core 14R09 (74.61°N, 168.98°W; 33 cm long but only the upper 13 cm are analyzed, 184 m water depth) were recovered during the Chinese National Arctic Research Expedition (CHINARE) in 2014 on board the R/V Xuelong from the eastern and northern Chukchi Sea, respectively. Core LV77-4 (69.20°N, 174.9°W; 44 cm long, 60 m water depth) was retrieved from the southern Chukchi Sea during LV77 cruise on board the R/V Akademik M A Lavrentiev in 2016. The three cores were subsampled on-board at a 1 cm sampling step and stored frozen at −20°C until analyses in the laboratory.

2.2. Satellite and historical sea ice concentration (SIC) data and biomarker records compilation

Time series of observed monthly SIC (1850–2017) at each core site (averages shown in table 1) were extracted using the version 2 of the 0.25° × 0.25° grid monthly sea ice extent and concentrations of Walsh *et al* (2019) available at the National Snow and Ice Data Center (NSIDC; https://noaadata.apps.nsidc.org/NOAA/G10010_V2/). Monthly SIC data were retrieved from the nearest 0.25° of latitude and longitude grid using the latest version of Panoply (https://www.giss.nasa.gov/tools/panoply/). Seasonal SIC was calculated by averaging the corresponding months as in Belt 2018, e.g. April-May-June for spring and July-August-September for summer. Adjacent-averaging smoothing was then applied to the SIC data for comparison with our lower resolution records.

From 1979 onward, we used Walsh *et al* (2019) dataset that consists of monthly satellite passive microwave SIC data only. For the period that predates the satellite era (i.e. 1850–1978), SIC data in the Chukchi Sea are from whaling ship reports, from the Russian Arctic and Antarctic Research Institute and historical sea ice charts of the Danish Meteorological Institute (Walsh *et al* 2017). Due to the temporal and spatial heterogeneity of the data, in particular those from whaling ships (between 1850 and 1919), temporal interpolation and analog-based estimations have been applied (Walsh *et al* 2017), therefore resulting in larger uncertainties in the historical part of the dataset (Walsh *et al* 2019). However, historical SIC data are used here for comparison with our biomarker records and only long-term trends are discussed.

Available data of IP_{25}, HBI III and brassicasterol were compiled from our cores and eleven other sediment cores retrieved from the pan Arctic Ocean (table 1). Only records strictly meeting selection criteria, i.e. dating

based on ^{210}Pb and ^{137}Cs and overlapping with the satellite era with at least one data point, are considered here. We also compiled the same proxy data from over 590 non-dated surface sediments in the sub-Arctic and Arctic regions for comparison with dated sediment calibrations (tables S1 and S2). Satellite SIC data at each core site in table 1 were obtained from Walsh *et al* (2019) dataset. For non-dated surface sediments, the satellite passive microwave SIC data are those provided in the original publications (Xiao *et al* 2015, Smik *et al* 2016, Kolling *et al* 2020, Koch *et al* 2020, Bai et al. 2024, Su *et al* 2023) (tables S1 and S2).

3. Methods

3.1. Core dating

The age models of the three cores are based on ^{210}Pb and ^{137}Cs measurements. The age models of cores 14S03 and 14R09 have been published by Astakhov *et al* (2019). For core LV77-4, the ^{210}Pb and ^{137}Cs measurements were performed at the State Key Laboratory of Estuarine and Coastal Research, East China Normal University, Shanghai, China, using an HPGe gamma spectrometry (GSW275L, Canberra). $^{210}Pb_{xs}$ was determined by subtracting the activity supported by its parent isotope, ^{226}Ra, from the total ^{210}Pb activity in the sediments. Errors in $^{210}Pb_{xs}$ were calculated by propagation of errors in the corresponding pair (^{226}Pa and ^{210}Pb).

3.2. Total organic carbon analysis

For total organic carbon (TOC) about 0.5 g of freeze-dried and homogenized sediment was acidified using 1 mol L^{-1} HCl and heated in a water bath for over three days to remove carbonates. Samples were then washed three times using ultrapure water and placed in an oven at 60°C until complete dryness. About 4 mg was then placed into a silver capsule and analyzed for TOC on an Elementar CHNOS elemental analyzer coupled with an isotope ratio mass spectrometer (IRMS) Thermo, Delta V advantage. These analyses were undertaken at the Key Laboratory of Marine Ecosystem Dynamics, Second Institute of Oceanography, Ministry of Natural Resources (MED, SIO, MNR, Hangzhou, China). Urea (with carbon wait of 20%) was used as a standard for TOC measurements. Based on replicate analyses, the analytical error was estimated to 0.1%.

3.3. Biomarker analyses

Between 2 and 4 g of freeze-dried and homogenized sediments were used to extract lipids in a mixture of dichloromethane/methanol (2:1 v/v). A known amount of internal standard 7-hexylnonadecane was added to the sediments before extraction for HBIs quantitation. Extraction and biomarker separation into compound classes by silica gel chromatography were performed following the procedure described in Ternois *et al* (2000). The hydrocarbon fraction, containing the HBIs, and the sterols were analyzed using a gas chromatograph Agilent Technologies 7890 (30 m HP-1MS column, 0.25 mm in diameter, and 0.25 μm film thickness) coupled to mass spectrometry Agilent 262 Technologies 5975C inert XL (GCMS). An external standard 5α-cholestane was added prior to GCMS analysis for the determination of sterol concentrations. For HBIs, the oven temperature was ramped from 40 °C to 300 °C, with a heating rate of 10 °C min^{-1}, and held at 300 °C for 10 min. For sterols, the GC oven temperature was programmed from 50 °C to 100 °C (at 30 °C min^{-1}), then from 100 °C to 150 °C (at 1.5 °C min^{-1}) and then from 150 °C to 300 °C (at 3 °C min^{-1}) and maintained for 20 min at 300 °C. Detection of HBIs and sterols was achieved using selective ion monitoring mode based on mass spectral responses of selected ions (m/z 350 for IP_{25}, m/z 348 for HBI II, m/z 346 for HBI III, m/z 470 for brassicasterol and m/z 500 for dinosterol). The same is done for the two standards; 7-hexylnonadecane (m/z 266) and 5α-cholestane (m/z 372). The relative abundances of biomarkers were determined by comparing their peak areas to those of the added standards. The concentrations were then normalized to dried sediment weights and TOC.

The PIP_{25} indexes were calculated using the following equation (1) (Müller *et al* (2011):

$$PIP_{25} = \frac{[IP_{25}]}{[IP_{25}] + [phytoplankton\ biomarker]_{*}c} \quad (1)$$

Where c is the balance factor calculated from biomarker concentrations of each core using equation (2) below:

$$c = \frac{mean\ IP_{25}\ concentration}{mean\ phytoplankton\ biomarker\ concentration} \quad (2)$$

H-Print was calculated using equation (3) below based on the peak areas of IP_{25}, HBI II and HBI III as determined by the GC-MS:

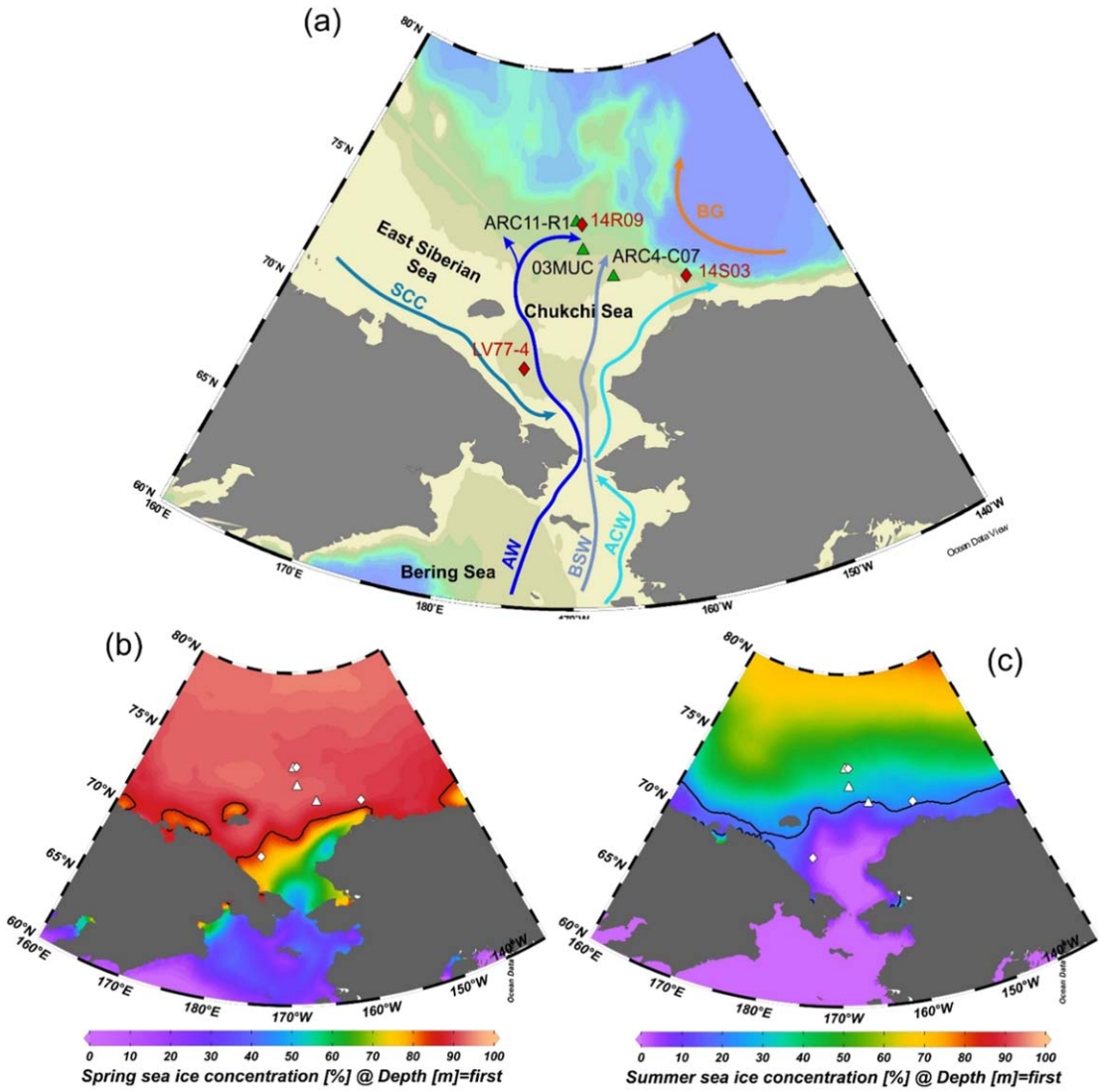

Figure 1. (a) Map showing the location of the studied cores (red diamonds) and sites where HBIs and sterols records covering the Industrial Era have been produced (green triangles); core ARC11-R1 (Su *et al* 2023), core ARC4-C07 (Bai *et al* 2022) and core ARA01B-03MUC (Kim *et al* 2019). Main water currents and Beaufort Gyre are also shown. (b) Spring (April, May and June) and (c) summer (July, August and September) averaged sea ice concentrations from 1994 to 2014 (http://nsidc.org). AW: Anadyr Water; BSW: Bering Sea Water; ACW: Alaska Costal Water; SCC: Siberian Costal Water; BG: Beaufort Gyre.

$$H - Print\% = \frac{[HBI - III]}{[IP_{25}] + [HBI - II] + [HBI - III]} \times 100 \quad (3)$$

4. Results

4.1. Chronology

Based on the ^{210}Pb and ^{137}Cs data published in Astakhov *et al* (2019), the sedimentation rates of cores 14R09 and 14S03 are estimated to be 0.044 cm yr^{-1} and 0.16 cm yr^{-1}, respectively. Assuming constant sedimentation rates, we found that 14S03 covers a period ranging from 1698 to 2005 and core 14R09 from 1707 to 1980. Note that the difference between the coring date (2014) and the core-top age is due to the missing top 1 cm for the two cores.

The $^{210}Pb_{xs}$ profile of core LV77-4 shows a nearly exponentially downcore decrease (figure S1; table S3). However, four $^{210}Pb_{xs}$ measurements show reversal and/or low values and high error bars and have thus been excluded from the log-linear $^{210}Pb_{xs}$ profile. Using the constant flux/constant sedimentation model, the mean sedimentation rate is estimated to 0.24 cm yr^{-1} ($R^2 = 0.93$), which is consistent with a more coastal location of this core. The ^{137}Cs peaks in the early 60s and late 80s, are also consistent with the $^{210}Pb_{xs}$ profiles. Based on the sedimentation rate value of 0.24 cm yr^{-1}, we calculated that core LV77-4 spans from 1827 to 2014.

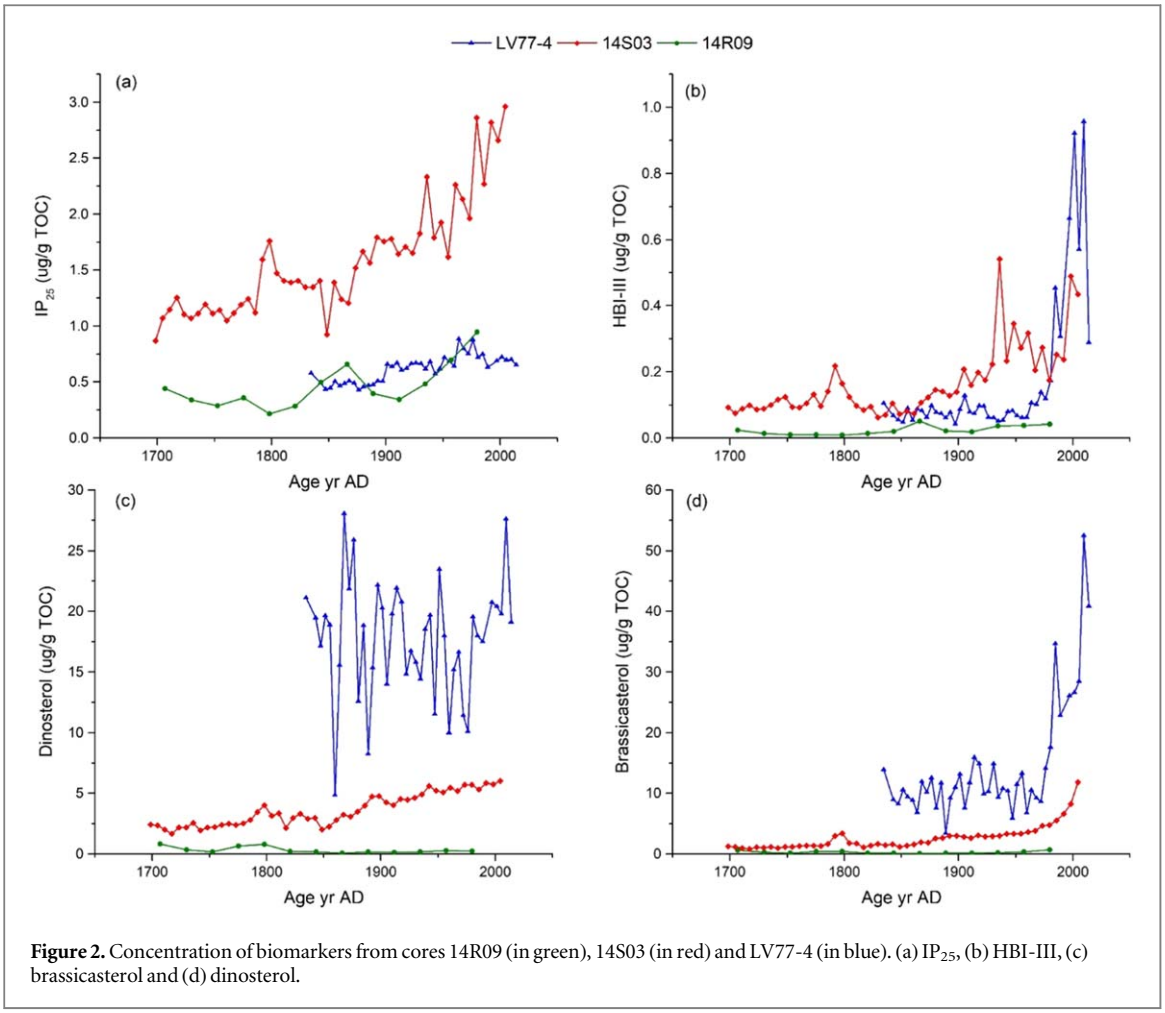

Figure 2. Concentration of biomarkers from cores 14R09 (in green), 14S03 (in red) and LV77-4 (in blue). (a) IP_{25}, (b) HBI-III, (c) brassicasterol and (d) dinosterol.

4.2. TOC downcore records

The TOC values vary between 0.59% and 0.91% in the northern core 14R09 (mean: 0.67%) (table S4). Higher values are found in the southern core LV77-4, ranging from 1.79% to 2.3% (mean: 2.02%), and intermediate ones in the eastern core 14S03 ranging from 1.42% to 2.3%, with a mean value of 1.65%. All three TOC profiles exhibit increase towards present but at different rates (figure S2).

4.3. HBIs and sterol downcore records

IP_{25} is detected throughout the three cores indicating the presence of seasonal sea ice (figure 2(a); table S4). The lowest IP_{25} values are found in the northern core 14R09 (from 0.22 to 0.95 $\mu g\, g^{-1}$ TOC; mean: 0.46 $\mu g\, g^{-1}$ TOC) and southern core LV77-4 (from 0.42 to 0.88 $\mu g\, g^{-1}$ TOC; mean: 0.61 $\mu g\, g^{-1}$ TOC) while they are significantly higher at the eastern 14S03 site (from 0.87 to 2.96 $\mu g\, g^{-1}$ TOC; mean: 1.58 $\mu g\, g^{-1}$ TOC) and show a sharp increase since 1850, which is less pronounced and delayed at 14R09, taking off at around 1900 (figure 2(a)). In contrast, IP_{25} in LV77-4 shows a modest increase with a short interval of slightly higher values between 1960 and the mid-1980s (figure 2(a)). IP_{25} and HBI II in the three cores show similar behavior, though with more scatter at LV77-4, in agreement with previous findings (Brown *et al* 2014) (figure S3). Pelagic phytoplankton biomarkers are generally low at the northern core 14R09, higher at 14S03 and even more at LV77-4 (figures 2(b), (c) and (d); tables S4). HBI III also show the lowest values at the northern core 14R09. Pelagic phytosterols increase towards present except for the northern core and for dinosterol in LV77-4 that display a strong variability with no clear rising trend. Interestingly, HBI III and brassicasterol in core LV77-4 show a drastic rise since the 1970s while IP_{25} remains rather stable (figures 2(a), (b) and (d)).

5. Discussion

5.1. Uncertainties related to sedimentation rate

The sedimentation rate at core 14R09 is low and in the range of earlier reports in nearby cores, i.e. 0.09 cm yr^{-1} (Kim *et al* 2019), 0.07 cm yr^{-1} (Su *et al* 2023) and 0.09 cm yr^{-1} (Bai *et al* 2022). At 14S03 and LV77-4,

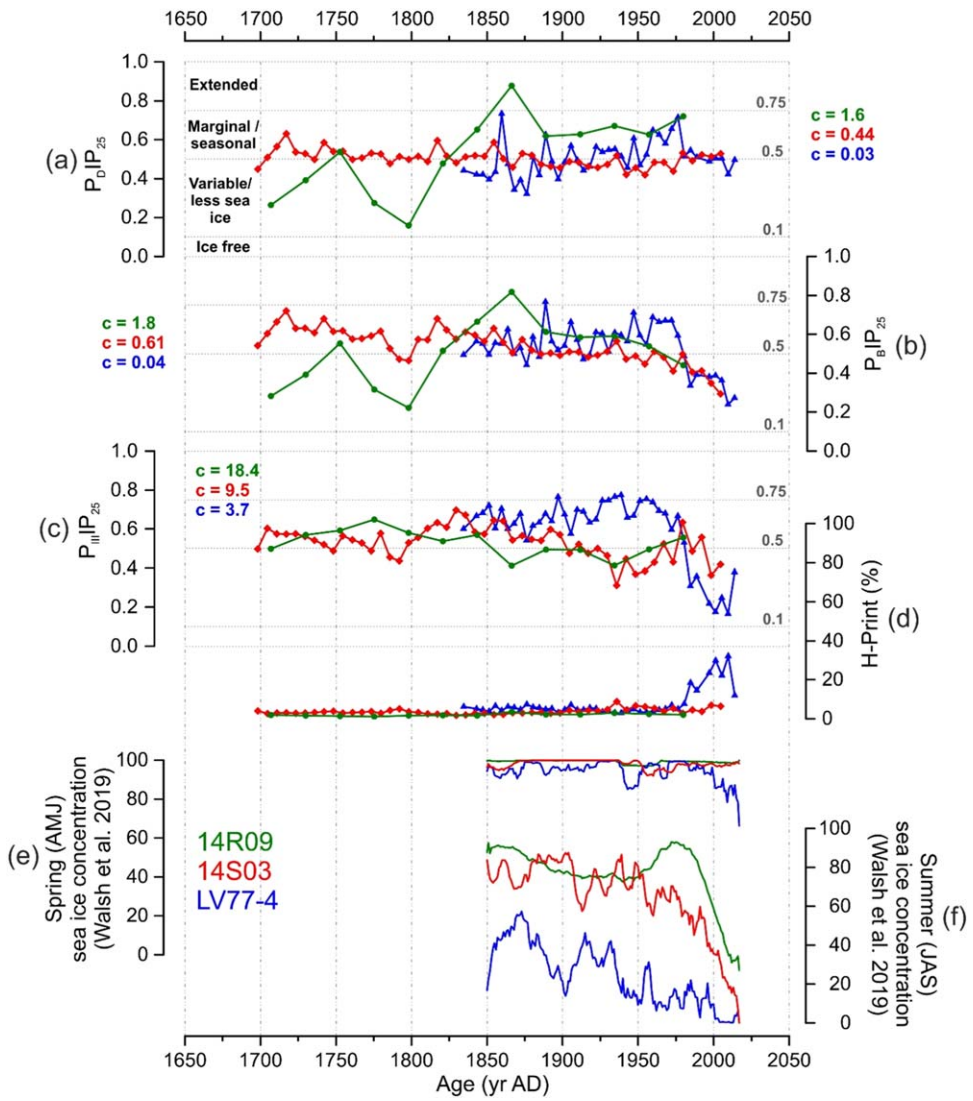

Figure 3. Downcore profiles from the three core sites (14R09 in green, 14S03 in red and LV77-4 in blue) of (a) P_DIP_{25}, (b) P_BIP_{25}, (c) P_{III}-IP_{25} and (d) H-Print (%). Horizontal dotted lines in (a), (b) and (c) indicate the boundaries of sea ice conditions as defined by Müller *et al* (2011): Ice free conditions (0 to 0.1), variable/less sea ice (0.1 to 0.5), marginal to seasonal sea ice (0.5 to 0.75) and extensive sea ice (0.75 to 1). (e) Spring (April-May-June) and (f) summer (July-August-September) sea ice concentrations at the core sites from historical and satellite data (Walsh *et al* 2019). For (e) and (f), the same coding color is used and 25-years, 7-years and 4-years adjacent-averaging smoothing are applied for data corresponding to 14R09, 14S03 and LV77-4, respectively, to fit the time-resolution of each core.

sedimentation rates fall into the range of 0.03 to 0.37 cm yr^{-1} reported for the Chukchi Shelf by Cooper and Grebmeier (2018). Although bioturbation and physical reworking of sediments cannot be ruled out (Cooper and Grebmeier 2018), the steady decline in $^{210}Pb_{ex}$ profiles in the three cores and the presence of the ^{137}Cs peak capturing the nuclear tests in the 60s in core LV77-4 (figures S1 and 2 in Astakhov *et al* 2019) suggest that sedimentation was not significantly affected by post-depositional processes. This finding is also consistent with the depth (60, 172 and 184 m) and geographical location of these sites far from areas highly influenced by bioturbation and water currents as testified by the radionuclide inventories of Cooper and Grebmeier (2018).

5.2. Reconstruction of sea ice conditions in the Chukchi Sea

5.2.1. Regional and temporal changes of biomarkers

The co-occurrence of sympagic HBIs (IP_{25} and HBI II) and pelagic phytoplankton biomarkers (HBI III, brassicasterol and dinosterol) throughout the three cores establishes the presence of seasonal sea ice as far back as the 1700s (figure 2) in agreement with previous studies in the northern Chukchi Sea (Kim *et al* 2019, Bai *et al* 2022, Su *et al* 2023) (figure 1(a)). The onset of the progressive increase of IP_{25} around 1850–1900 agrees with the beginning of summer sea-ice retreat reported in historical and observational data (Perovich *et al* 2019, Walsh *et al* 2019) (figures 2(a) and 3(f)) suggesting that shrinking sea ice and thinner snow cover favored sympagic production and export to the sea floor. The very low concentrations of sterols and H-Print (%) in the northern

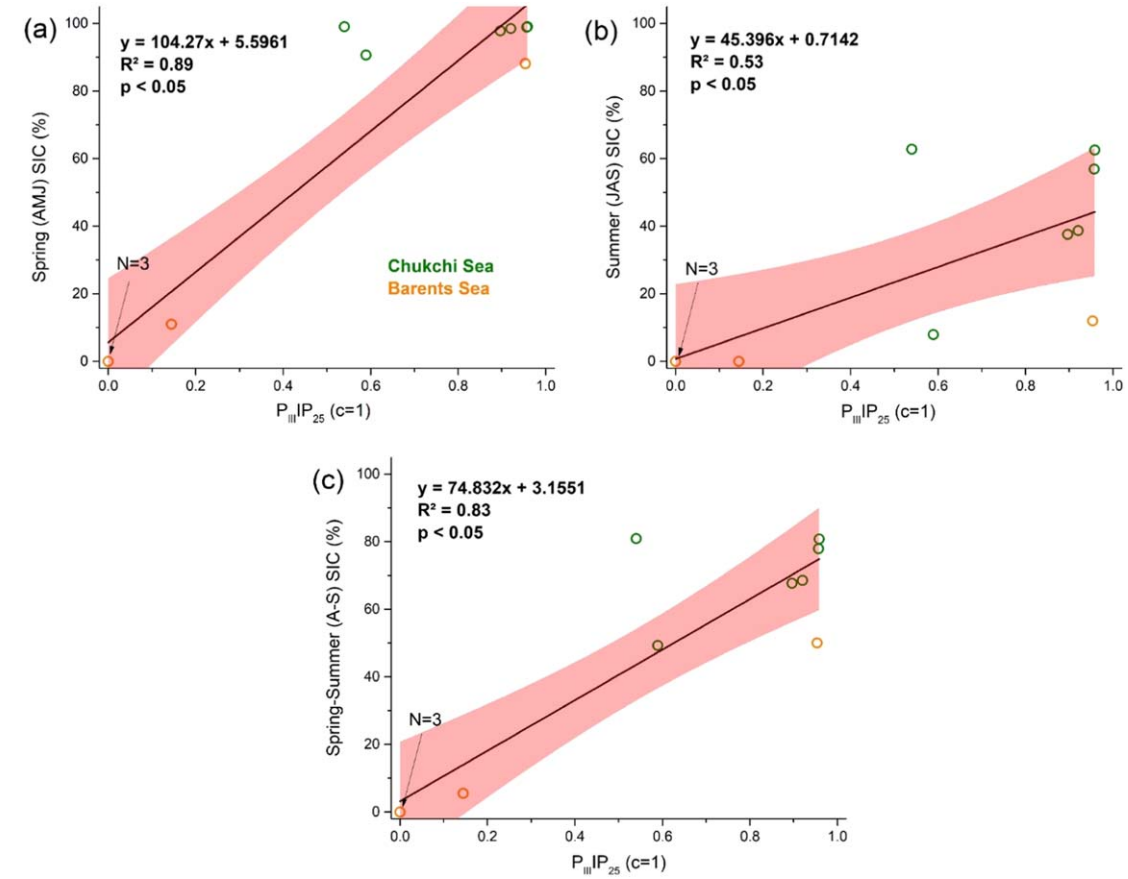

Figure 4. Correlation of $P_{III}IP_{25}$ from 11 sediment core-tops with (a) spring (April-May-June), (b) summer (July-August-September) and (c) spring-summer (April to September) sea ice concentration derived from satellite data (Walsh *et al* 2019). Thick black line represents the linear regression and the red band indicates the confidence level at 95%. The correlation coefficient R^2, p-value as well as the equation linking the $P_{III}IP_{25}$ to the SIC are shown for each correlation.

core 14R09 underline the dominance of sympagic production at 74.6° latitude (figures 2(c), (d) and 3(d)). At 14S03, sea ice algal production is highest but pelagic algal production is also high most likely reflecting sea ice edge conditions as pointed out by rising and high HBI III values (figure 2(b)). In core LV77-4, the sharply increase of pelagic HBI III and brassicasterol (figure 2(b), (d)) as well as H-Print (%) (figure 3(d)) during the last decades indicate a drastic increase of pelagic phytoplankton production in summer (Perovich *et al* 2019, Frey *et al* 2021). Note that dinosterol diverges from this trend and instead shows a strong variability. All together, these results feature the northward increase of sympagic versus pelagic algal production as expected from retreating sea ice in agreement with summer sea ice observations between 1994 and 2014 at the three sites (figure 1(c)) and previous reconstructions of Koch *et al* (2020) and Su *et al* (2023) based on surface sediments and short cores.

5.2.2. Semi-quantitative estimates of sea ice cover in the Chukchi Sea

PIP_{25} indexes (P_DIP_{25}, P_BIP_{25} and $P_{III}IP_{25}$) were calculated to derive semi-quantitative estimates of sea ice cover at our sites (figures 3(a), (b) and (c)) (table S4). At the northern 14R09 site the three indexes translate into different patterns. $P_{III}IP_{25}$ values (ranging between 0.5 and 0.75, figure 3(c)) indicate relatively stable conditions over the last 300 years corresponding to marginal to seasonal sea ice (Müller *et al* 2011) while P_DIP_{25} (figure 3(a)) show increase sea ice. Only P_BIP_{25} (figure 3(b)) broadly reproduce the summer sea ice decline seen in the historical and satellite data since 1850 (figure 3(f), Walsh *et al* 2019). Comparison with previously published data from a nearby site 03MUC in the northern Chukchi Sea published by Kim *et al* (2019) indicate similarities for P_BIP_{25} and $P_{III}IP_{25}$ and to a lesser extent with P_DIP_{25} (figure S4).

In the eastern Chukchi Sea, core 14S03 under the influence of the Alaska Costal Water (ACW, figure 1), the three indexes indicate marginal (0.5 to 0.75) to variable sea ice conditions (0.1 to 0.5) throughout the core (figures 3(a), (b) and (c)). Again, P_BIP_{25} seems to better reproduce the summer sea ice decline documented by the historical and satellite data until 2000 than P_DIP_{25} and $P_{III}IP_{25}$.

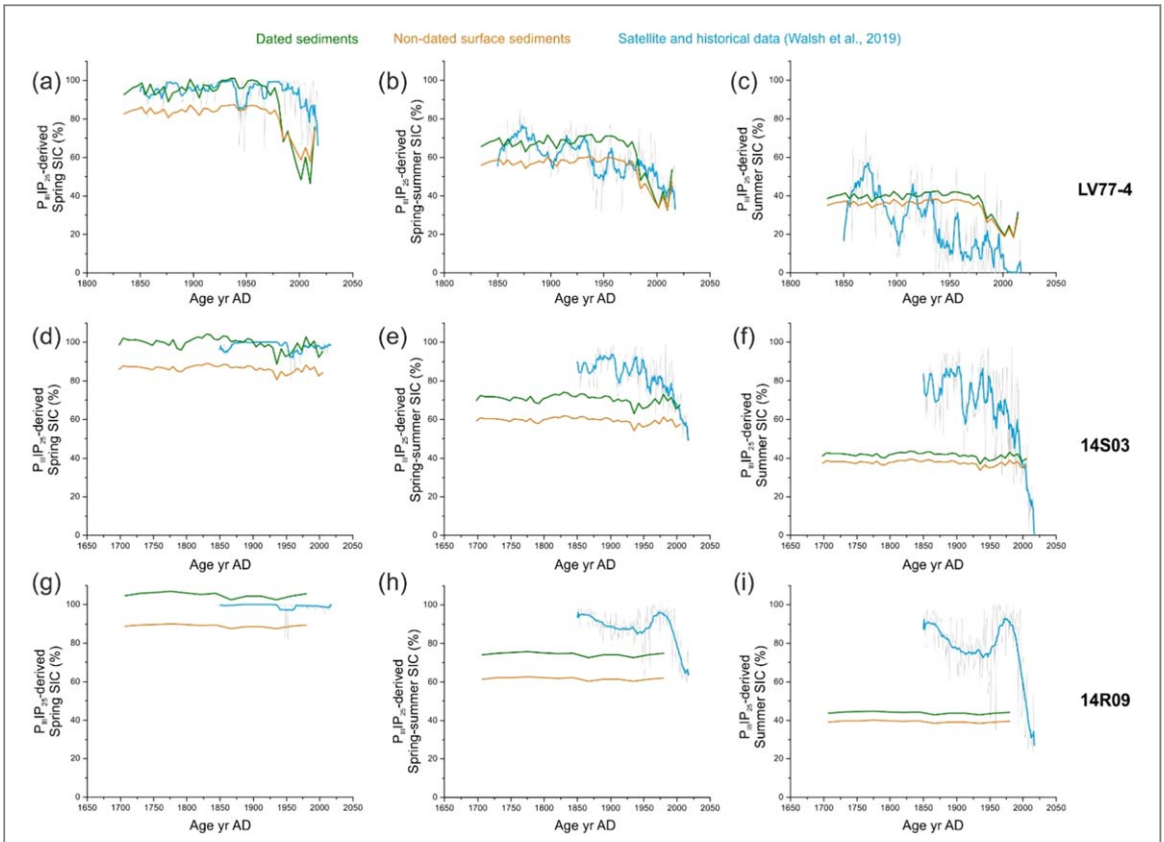

Figure 5. $P_{III}IP_{25}$-derived spring (AMJ; left column), spring-summer (A-S; middle column) and summer (JAS; right column) sea ice concentration from cores LV77-4 (a, b and c), 14S03 (d, e and f) and 14R09 (g, h and i) sites using calibrations shown in figure 4 (in green) and those from non-dated surface sediments shown in figure S6B (in orange). The same seasonal sea ice concentration from historical and satellite data at each core site (Walsh *et al* 2019) are also shown for comparison (blue lines represent adjacent-averaging smoothing that corresponds to the temporal-resolution of each core).

At the southern site LV77-4, the three PIP_{25} indexes indicate marginal to seasonal sea ice conditions from 1830 to the 1950s (figures 3(a), (b) and (c)). Only P_BIP_{25} seems to reflect the decrease of summer sea ice cover and to some extent spring sea ice seen in the satellite and historical data (figures 3(e), (f)), when sea ice starts breaking out.

Overall our results suggest that P_BIP_{25} better match remote sensing and historical data of summer sea ice at the northern and eastern sites when sea ice breakdown (Bai *et al* 2019) and to some extent also with spring sea ice cover at the southern site, where melting occurs earlier.

5.3. PIP_{25}-derived SIC: insight from remote sensing and proxy data correlation

PIP_{25} indexes have been often calibrated against satellite data to then reconstruct SIC in the Arctic prior to the instrumental period (Xiao *et al* 2015, Smik *et al* 2016, Kolling *et al* 2020, Bai *et al* 2022). In this approach, biomarker data have been generally measured in surface sediments retrieved from different sea ice settings across the Arctic Ocean (Kolling *et al* 2020) but, as highlighted by Xiao *et al* (2015), the sediments are often poorly or not dated and thus represent different time spans ranging from several years to hundreds of years depending on the sedimentation rates.

To reduce biases linked to time uncertainties and improve the proxy calibration against observed SIC, we used here our ^{210}Pb-dated P_BIP_{25} and $P_{III}IP_{25}$ dataset and combined them with published ^{210}Pb-dated sediment records overlapping the remote sensing period (table 1; figure S5) (Köseoğlu *et al* 2018, Belt *et al* 2019, Kim *et al* 2019, Bai *et al* 2022, Su *et al* 2023, Davies et al. 2024). Only sediment cores recovered in Arctic marginal seas (Chukchi, Greenland and Barents seas) with high sedimentation rate and seasonal sea ice were considered (table 1).

$P_{III}IP_{25}$ records meeting these criteria are from five sediment cores from the Barents Sea (Köseoğlu *et al* 2018, Belt *et al* 2019) and six sediment cores from the Chukchi Sea (including our three cores, Kim *et al* 2019, Bai *et al* 2022, Su *et al* 2023) (table 1; figure S5a). For P_BIP_{25}, in addition to six cores from the Chukchi Sea, we used recently published data from three short cores off NE Greenland (Davies et al. 2024) (figure S5b). All $P_{III}IP_{25}$ and P_BIP_{25} data are calculated using a balance factor c = 1 and using c calculated from biomarker data of each core, respectively. At each core site, PIP_{25} values are averaged over the time-interval of the remote sensing

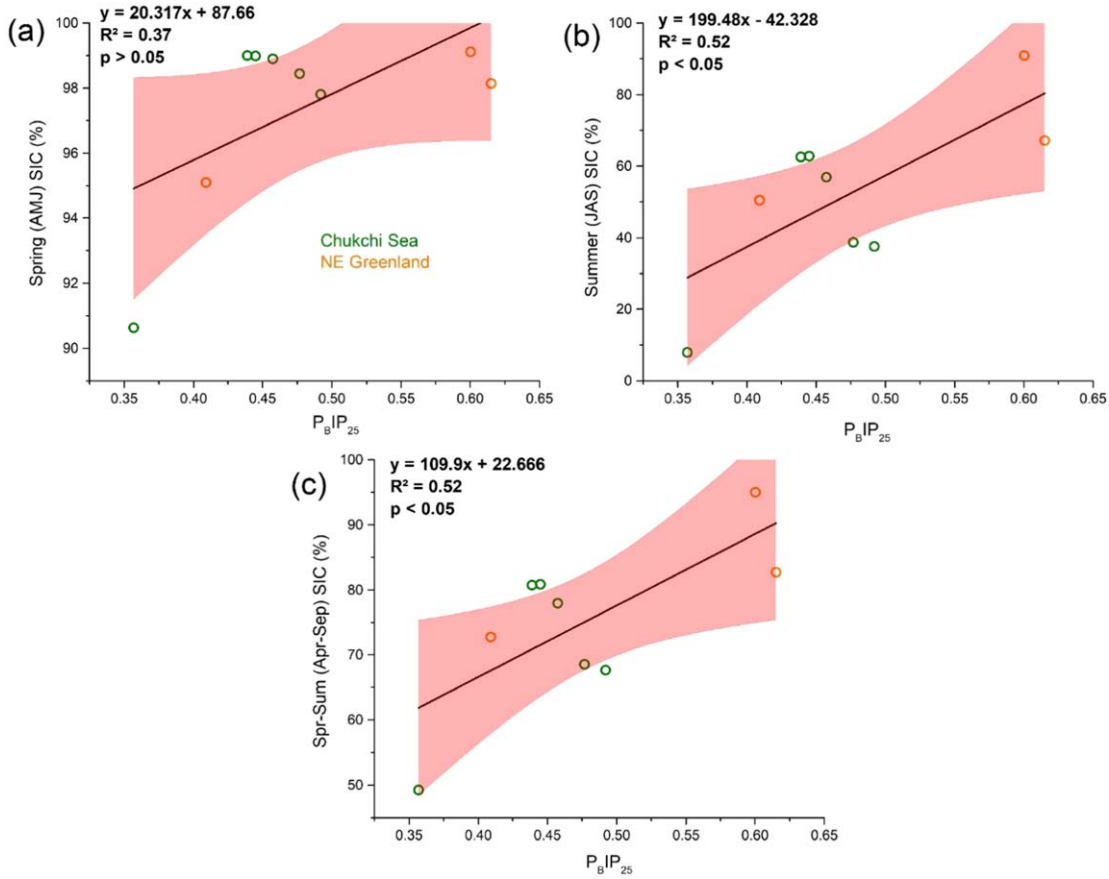

Figure 6. Correlation of P_BIP_{25} from 9 sediment core-tops with (a) spring (April-May-June), (b) summer (July-August-September) and (c) spring-summer (April to September) sea ice concentration derived from satellite data (Walsh *et al* 2019). Thick black line represent the linear regression while red band indicates the confidence level at 95%. The correlation coefficient R^2, p-value as well as the equation linking the P_BIP_{25} to the SIC are shown for each correlation.

period (from 1979 to the most recent data point) to one single value. The same is done at each core site for satellite SIC data obtained from Walsh *et al* (2019) (table 1). Linear correlations are then calculated from PIP_{25} (P_BIP_{25} and $P_{III}IP_{25}$) and satellite SIC for summer (SuSIC), spring (SpSIC) and average of these two seasons (Sp-SuSIC). For the non-dated surface sediments of the pan-Subarctic and Arctic regions, the compilation of $P_{III}IP_{25}$ and P_BIP_{25} data are given in table S1 and S2, respectively (Xiao *et al* 2015, Smik *et al* 2016, Kolling *et al* 2020, Koch *et al* 2020, Su *et al* 2022, Bai et al. 2024). The same linear correlations between PIP_{25} from non-dated surface sediments and satellite SIC are calculated for comparison with dated sediment calibrations (figure S6).

The $P_{III}IP_{25}$ shows significant correlation with both SuSIC (JAS) and SpSIC (AMJ) with R^2 of 0.53 and 0.89, respectively ($p < 0.01$; figures 4(a), (b)). For Sp-SuSIC, the correlation is 0.83 ($p < 0.01$) (figure 4(c)). Figure 5 shows the downcore profiles of $P_{III}IP_{25}$-derived SpSIC, SuSIC and Sp-SuSIC in our three sediment cores using the new calibrations as well as that based on non-dated surface sediments and the modern observations (Walsh *et al* 2019). $P_{III}IP_{25}$-derived SpSIC indicates high values at the three core sites, with only few ones exceeding 100%, that however agrees with historical and satellite data during the overlapped period (figures 5(a), (d) and (g)). $P_{III}IP_{25}$-derived Sp-SuSIC indicates relatively good correspondence with historical and satellite data except for the northern site becoming less accurate moving northwards (figures 5(b), (e), (h)). Reconstructions perform even less to reproduce Su-SIC (figures 5(c), (f) and (i)). These results reflect the higher correlation between $P_{III}IP_{25}$ and SpSIC than with SuSIC (figures 4(a), (b)) and the higher export of HBI III in late spring-early summer from surface waters evidenced by Bai *et al* (2019) under sea ice edge conditions. Comparison of $P_{III}IP_{25}$-derived SpSIC, Sp-SuSIC and SuSIC using the non-dated sediment-based calibration (figure S6B) indicates that SIC are almost always underestimated compared to historical and satellite data (figure 5).

P_BIP_{25} values from 9 dated sediment cores indicate significant correlation with SuSIC and Sp-SuSIC (figure 6). Contrary to the $P_{III}IP_{25}$, P_BIP_{25} values do not show a significant correlation with SpSIC but with SuSIC as evidenced in the previous section (figures 6(a), (b)). P_BIP_{25}-derived SpSIC, SuSIC and Sp-SuSIC generally agree with historical and satellite time series but less for the southern site where $P_{III}IP_{25}$ better matched (figure 7). The P_BIP_{25}-derived SpSIC indicates extensive sea ice conditions with SIC values close to 100% at the

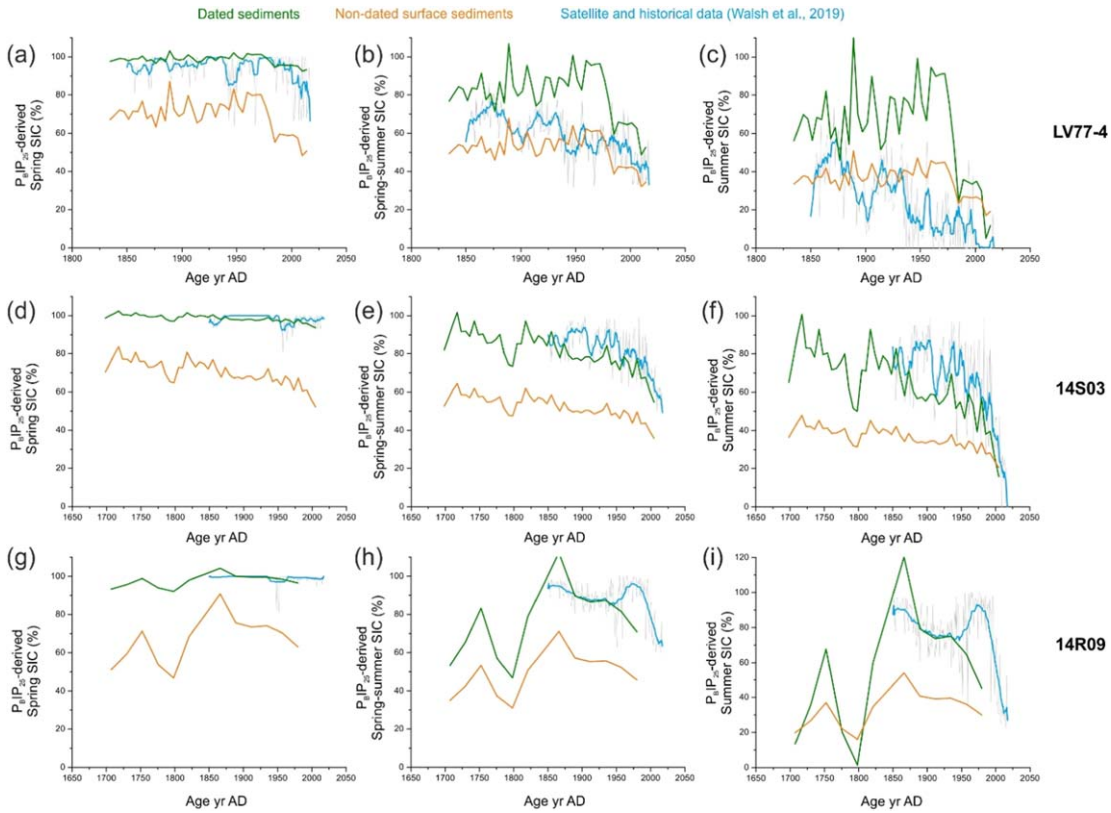

Figure 7. P_BIP_{25}-derived spring (AMJ; left column), spring-summer (A-S; middle column) and summer (JAS; right column) sea ice concentration from cores LV77-4 (a, b and c), 14S03 (d, e and f) and 14R09 (g, h and i) using calibrations shown in figure 6 (in green) and those from non-dated surface sediments shown in figure S6A (in orange). The same seasonal sea ice concentration from historical and satellite data at each core site (Walsh *et al* 2019) are also shown for comparison (blue lines represent adjacent-averaging smoothing that corresponds to the temporal-resolution of each core).

three core sites in good correspondence with the historical and satellite data (figures 7(a), (d) and (g)). However, SuSIC from core 14R09 yields lower values during the pre-industrial period due to relatively high values of brassicaterol that may be explained by diatoms production below the sea ice (Coupel *et al* 2012) (figure 7(i)). Moreover, data from core LV77-4 broadly overestimate the SuSIC and Sp-SuSIC compared to the historical and satellite data with few values slightly exceeding 100% (figures 7(b), (c)), a result that might be explained by advection of sea ice. Indeed, Su *et al* (2023) suggested that in this coastal area track drifting and land-fast ice may contribute to the sedimentary HBIs, and possibly account for the HBI II profile diverging from IP_{25} in this core. Similar to $P_{III}IP_{25}$-derived SIC, reconstructions based on P_BIP_{25} from non-dated surface sediments broadly underestimate SIC compared to those reconstructed using dated sediment-based calibrations and to historical and satellite data (figure 7). Overall our study shows that dated sediments contribute to improve the statistical relationship between PIP_{25} and observations and subsequently the quantitative estimates of past changes of SIC beyond the Satellite Era.

6. Conclusions

Biomarker records of IP_{25}, HBI II, HBI III, brassicasterol and dinosterol, were generated from three new sediment cores recovered in the northern, eastern and southern Chukchi Sea to reconstruct sea ice conditions beyond the Industrial Era (since 1700). PIP_{25} and H-Print evidence dominant sympagic over pelagic production at the three core sites and a sharp increase of pelagic phytoplankton production at the more coastal southern core over the last decades.

Our study demonstrates that the compilation of dated sediments improves calibrations between PIP_{25} index and satellite data and provides statistically stronger relationships between $P_{III}IP_{25}$ and SpSIC and between P_BIP_{25} and SuSIC. Application of the new calibrations to the downcore PIP_{25} records results in a better degree of agreement between SIC estimates and historical and satellite time series. In particular, our results show that P_BIP_{25} reproduce SuSIC in historical and satellite data at the two northern cores while $P_{III}IP_{25}$ better reflects SpSIC in the southernmost site, as expected from the export pattern of HBI III in late spring-early summer evidenced from sediment trap time series.

Acknowledgments

This study was funded by the National Natural Science Foundation of China (Nos. 41941013, 41606052) and the Scientific Research Fund of the Second Institute of Oceanography, MNR, grand no. JB2404. The LV77 cruise was partly supported by the Ministry of Sciences and Education of the Russian Federation (project no. 124022100084-8). We are grateful to Qianna Chen and Jiaqi Wu of the Second Institute of Oceanography for their kind help in the bulk and biomarker measurements. We thank the Centre National de la Recherche Scientifique for salary support of MAS and VK.

Data availability statement

All data that support the findings of this study are included within the article (and any supplementary files).

ORCID iDs

Bassem Jalali https://orcid.org/0000-0002-4171-1664
Marie-Alexandrine Sicre https://orcid.org/0000-0002-5015-1400
Jian Ren https://orcid.org/0000-0002-1889-5661
Jianfang Chen https://orcid.org/0000-0002-6521-0266

References

Abram N J, McGregor H V, Tierney J E, Evans M N, McKay N P and Kaufman D S 2016 Early onset of industrial-era warming across the oceans and continents *Nature* **536** 411–8

Astakhov A S, Bosin A A, Liu Y G, Darin A V, Kalugin I A, Artemova A V and Vologina E G 2019 Reconstruction of ice conditions in the northern Chukchi Sea during recent centuries: geochemical proxy compared with observed data *Quat. Int.* **522** 23–37

Bai Y, Sicre M A, Chen J, Klein V, Jin H, Ren J and Zhao M 2019 Seasonal and spatial variability of sea ice and phytoplankton biomarker flux in the Chukchi sea (western Arctic Ocean) *Prog. Oceanogr.* **171** 22–37

Bai Y, Sicre M A, Ren J, Jalali B, Klein V, Li H and Chen J 2022 Centennial-scale variability of sea-ice cover in the Chukchi Sea since AD 1850 based on biomarker reconstruction *Environ. Res. Lett.* **17** 044058

Bai Y, Sicre M-A, Ren J, Klein V, Jin H and Chen J 2024 Latitudinal distribution of biomarkers across the western Arctic Ocean and the Bering Sea: an approach to assess sympagic and pelagic algal production *Biogeosciences* **21** 689-709

Ballinger T J, Overland J E, Wang M, Bhatt U S, Hanna E, Hanssen-Bauer I and Walsh J E 2020 *Surface air temperature* Arctic report card 1–7

Belt S T, Massé G, Rowland S J, Poulin M, Michel C and LeBlanc B 2007 A novel chemical fossil of palaeo sea ice: IP25 *Org. Geochem.* **38** 16–27

Belt S T 2018 Source-specific biomarkers as proxies for Arctic and Antarctic sea ice *Organic Geochemistry* **125** 277–98

Belt S T, Smik L, Köseoğlu D, Knies J and Husum K 2019 A novel biomarker-based proxy for the spring phytoplankton bloom in Arctic and sub-arctic settings–HBI T25. *Earth Planet. Sci. Lett.* **523** 115703

Bernstein L, Bosch P, Canziani O, Chen Z, Christ R and Riahi K 2008 *IPCC, 2007: Climate Change 2007: Synthesis Report. Contribution of Working Groups I, II and III to the Fourth Assess- ment Report of the Intergovernmental Panel on Climate Change* IPCC, Geneva, Switzerland 104 pp

Brown T A, Belt S T, Tatarek A and Mundy C J 2014 Source identification of the Arctic sea ice proxy IP25 *Nat. Commun.* **5** 4197

Cooper L W and Grebmeier J M 2018 Deposition patterns on the Chukchi shelf using radionuclide inventories in relation to surface sediment characteristics *Deep Sea. Res. Part II* **152** 48–66

Coupel P, Ruiz-Pino D, Sicre M-A, Chen J, Lee S, Schiffrine N, Li H and Gascard J-C 2015 The impact of freshening on phytoplankton production in the Pacific Arctic Ocean Prog *Oceanogr.* **131** 113–25

Coupel P, Jin H Y, Joo M, Horner R, Bouvet H A, Sicre M A and Ruiz-Pino D 2012 Phytoplankton distribution in unusually low sea ice cover over the Pacific Arctic *Biogeosciences* **9** 4835–50

Davies J, Fahl K, Moros M, Carter-Champion A, Detlef H, Stein R, Pearce C and Seidenkrantz M-S 2024 Sea-ice conditions from 1880 to 2017 on the Northeast Greenland continental shelf: a biomarker and observational record comparison *The Cryosphere* **18** 3415–31

Frey K E, Comiso J C, Cooper L W, Grebmeier J M and Stock L V 2020 Arctic ocean primary productivity: the response of marine algae to climate warming and sea ice decline *Arctic Report Card* (https://doi.org/10.25923/vtdn-2198)

Hu L, Liu Y, Xiao X, Gong X, Zou J, Bai Y, Gorbarenko S, Fahl K, Stein R and Shi X 2020 Sedimentary records of bulk organic matter and lipid biomarkers in the Bering Sea: a centennial perspective of sea-ice variability and phytoplankton community *Mar. Geol.* **429** 106308

Calvin K *et al* 2023 *IPCC, 2023: Climate Change 2023: Synthesis Report. Contribution of Working Groups I, II and III to the Sixth Assessment Report of the Intergovernmental Panel on Climate Change [Core Writing Team, H. Lee and J. Romero (eds.)]. IPCC, Geneva, Switzerland.* IPCC, Geneva, Switzerland 1–34

Kapsch M L, Graversen R G, Tjernström M and Bintanja R 2016 The effect of downwelling longwave and shortwave radiation on Arctic summer sea ice *J. Clim.* **29** 1143–59

Kim J H, Gal J K, Jun S Y, Smik L, Kim D, Belt S T and Nam S I 2019 Reconstructing spring sea ice concentration in the Chukchi Sea over recent centuries: insights into the application of the PIP25 index *Environ. Res. Lett.* **14** 125004

Koch C W, Cooper L W, Lalande C, Brown T A, Frey K E and Grebmeier J M 2020 Seasonal and latitudinal variations in sea ice algae deposition in the Northern Bering and Chukchi Seas determined by algal biomarkers *PLoS One* **15** e0231178

Kolling H M, Stein R, Fahl K, Sadatzki H, de Vernal A and Xiao X 2020 Biomarker distributions in (sub)-Arctic surface sediments and their potential for sea ice reconstructions *Geochem. Geophys. Geosyst.* **21** e2019GC008629

Köseoğlu D, Belt S T, Husum K and Knies J 2018 An assessment of biomarker-based multivariate classification methods versus the PIP25 index for paleo Arctic sea ice reconstruction *Org. Geochem.* **125** 82–94
Kwok R and Rothrock D A 2009 Decline in Arctic sea ice thickness from submarine and ICESat records: 1958–2008 *Geophys. Res. Lett.* **36** L15501
Lee Y, Min J-O, Yang E J, Cho K-H, Jung J, Park J, Moon J K and Kang S-H 2019 Influence of sea ice concentration on phytoplankton community structure in the Chukchi and East Siberian Seas, Pacific Arctic Ocean *Deep-Sea Res. I* **147** 54–64
McCulloch M T, Winter A, Sherman C E and Trotter J A 2024 300 years of sclerosponge thermometry shows global warming has exceeded 1.5 °C *Nat. Clim. Change* **14** 1–7
Müller J, Wagner A, Fahl K, Stein R, Prange M and Lohmann G 2011 Towards quantitative sea ice reconstructions in the northern North Atlantic: a combined biomarker and numerical modelling approach *Earth Planet. Sc. Lett.* **306** 137–48
Ogi M, Yamazaki K and Wallace J M 2010 Influence of winter and summer surface wind anomalies on summer Arctic sea ice extent *Geophys. Res. Lett.* **37** L07701
Perovich D *et al* 2019 Sea Ice *Arctic Rep. Card* 2019 (https://doi.org/10.25923/n170-9h57)
Smik L, Cabedo-Sanz P and Belt S T 2016 Semi-quantitative estimates of paleo Arctic sea ice concentration based on source-specific highly branched isoprenoid alkenes: a further development of the PIP25 index *Org. Geochem.* **92** 63–9
Su L, Ren J, Sicre M A, Bai Y, Jalali B, Li Z and Chen J 2022 HBIs and sterols in surface sediments across the East Siberian Sea: implications for palaeo sea-ice reconstructions *Geochem. Geophys. Geosyst.* **23** e2021GC009940
Su L, Ren J, Sicre M A, Bai Y, Zhao R, Han X and Chen J 2023 Changing sources and burial of organic carbon in the Chukchi Sea sediments with retreating sea ice over recent centuries *Climate of the Past* **19** 1305–20
Ternois Y, Kawamura K, Ohkouchi N and Keigwin L 2000 Alkenone sea surface temperature in the Okhotsk Sea for the last 15 kyr *Geochem. J.* **34** 283–93
Timmermans M L and Labe Z 2020 Sea Surface Temperature *Arctic Report Card 2020* (https://doi.org/10.25923/v0fs-m920)
Tschudi M A, Stroeve J C and Stewart J S 2016 Relating the age of Arctic sea ice to its thickness, as measured during NASA's ICESat and IceBridge campaigns *Remote Sensing* **8** 457
van Westen R M, Kliphuis M and Dijkstra H A 2024 Physics-based early warning signal shows that AMOC is on tipping course *Sci. Adv.* **10** eadk1189
Walsh J E, Fetterer F, Scott Stewart J and Chapman W L 2017 A database for depicting Arctic sea ice variations back to 1850 *Geographical Review* **107** 89–107
Walsh J E, Chapman W L, Fetterer F and Stewart S 2019 *Gridded Monthly Sea Ice Extent and Concentration, 1850 Onward, Version 2* NSIDC: National Snow and Ice Data Center
Xiao X, Fahl K, Müller J and Stein R 2015 Sea-ice distribution in the modern Arctic Ocean: biomarker records from trans-Arctic Ocean surface sediments *Geochim. Cosmochim. Acta* **155** 16–29
Zhuang Y, Jin H, Chen J, Ren J, Zhang Y, Lan M, Zhang T, He J and Tian J 2020 Phytoplankton community structure at subsurface chlorophyll maxima on the western Arctic shelf: patterns, causes, and ecological importance *J. Geophys. Res. Biogeosci.* **125** e2019JG005570